Applied Catalysis B: Environmental 181 (2016) 587–598

Contents lists available at ScienceDirect

Applied Catalysis B: Environmental

journal homepage: www.elsevier.com/locate/apcatb

Kinetic study of adsorption and desorption of SO_2 over γ-Al_2O_3 and Pt/γ-Al_2O_3

Tayebeh Hamzehlouyan[a], Chaitanya S. Sampara[a], Junhui Li[b], Ashok Kumar[b], William S. Epling[a,*]

[a] Department of Chemical and Biomolecular Engineering, University of Houston, Houston, TX, United States
[b] Catalyst Technology, Cummins Inc., Columbus, IN, United States

ARTICLE INFO

Article history:
Received 16 May 2015
Received in revised form 2 August 2015
Accepted 4 August 2015
Available online 13 August 2015

Keywords:
SO_2 adsorption
Sulfate decomposition
Diesel oxidation catalyst
Sulfur poisoning

ABSTRACT

SO_2 storage and release on/from γ-Al_2O_3 and Pt/γ-Al_2O_3 were studied in order to understand the transient phenomena that occur upon a diesel oxidation catalyst's (DOC) exposure to SO_2. Temperature programmed desorption (TPD) and in-situ diffuse reflectance infrared Fourier transform spectroscopy (DRIFTS) experiments were performed to understand the adsorption, surface reaction and desorption dynamics. Adsorption data verified that γ-Al_2O_3 as a catalyst support significantly affects the SO_2 storage and release of a Pt/γ-Al_2O_3 catalyst. Multiple sulfur species formed during SO_2 adsorption on γ-Al_2O_3 and Pt/γ-Al_2O_3. SO_2 adsorbed as molecular SO_2 on Al sites, as surface sulfites/bi-sulfites and surface sulfates on electron deficient oxygen sites, as well as bulk aluminum sulfate were identified. The results show that Pt has a promoting effect on surface sulfate formation as well as on spillover of surface sulfates into the bulk alumina support. Based on the DRIFTS and TPD studies, multi-step reaction mechanisms were proposed for SO_2 adsorption and desorption on/from both γ-Al_2O_3 and Pt/γ-Al_2O_3. The kinetic parameters were optimized to describe the TPD experimental data and the kinetic models were able to accurately predict the experimental behavior of the catalyst. Similar steady state coverage profiles were predicted by the model irrespective of inlet concentrations for long exposure times, suggesting that low SO_2 concentrations typically seen in diesel exhaust can be simulated with higher concentrations to accelerate the sulfur effects.

1. Introduction

The diesel oxidation catalyst (DOC) is a vital component of the diesel engine aftertreatment architecture and is used to oxidize CO and hydrocarbons to CO_2 and H_2O, and to oxidize NO to NO_2. It is relatively well known that sulfur is a common catalyst poison in automotive catalysis and can impact these oxidation functions. Sulfur compounds originating from fuel are released mostly in the form of SO_2 after combustion in the engine [1]. Complicating the effects, depending on the exhaust temperature, SO_2 can be oxidized to SO_3 over a DOC. SO_2 and SO_3 can have different impacts on the DOC and other downstream catalysts, with SO_3 leading to more severe deactivation, at least partly due to its affinity to form H_2SO_4.

The effects of SO_2 on CO, NO and hydrocarbon oxidation reactions over Pt/γ-Al_2O_3 catalysts have been previously studied [2–6]. Gracia et al. [2] found that in the presence of 20 ppm SO_2 in the feed, the CO light-off temperature on alumina- and silica-supported Pt increased by at least 20 °C. Site blocking as well as modification of Pt—CO bonding were reported as possible sulfur poisoning effects. Their results revealed that alumina acted as a sulfur storage reservoir, which could delay the appearance of catalyst deactivation [2]. Krocher et al. [4] studied sulfur deactivation of NO oxidation and according to their results, sulfation of DOCs is a two stage process, starting with oxidation of SO_2 to SO_3 and the adsorption of sulfuric acid at the surface, followed by a slower sulfation of the bulk washcoat. The NO oxidation activity decreased significantly in the presence of SO_2, due to the SO_x storage on the catalyst surface. The activity could be completely recovered upon heating the catalyst to 400 °C. Very stable sulfate species, which remained on the washcoat, were found to have a negligible effect on the NO oxidation performance [4]. In another study performed by Li et al. [6], the impact of SO_2 on the performance of Pt/Pd-based DOCs was investigated using NO and hydrocarbon oxidation as probe reactions. The authors showed that sulfur in its freshly deposited state directly interacts with the precious metal sites, leading to NO and hydrocarbon oxidation activity loss. With subsequent operation in

* Corresponding author.
E-mail address: wsepling@uh.edu (W.S. Epling).

http://dx.doi.org/10.1016/j.apcatb.2015.08.003
0926-3373/

Nomenclature

a_j	total active site density for reaction j (mol site·m^3)
$a_{j,Sk}$	active site density of site k for reaction j (mol site·m^{-3})
A	face area (m^2)
$\vec{c}_s$	vector of molar concentrations of trace species at catalyst surface (mol·m^{-3})
F	function to specify surface coverages (s^{-1})
r_j	rate of production of reaction j (mol·mol site^{-1} s^{-1})
s_{ij}	stoichiometric coefficient of species i in reaction j
t	time (s)
T_g	temperature of bulk gas phase (K)
T_s	temperature of solid phase (K)
w_{in}	inlet molar flow rate (mol·s^{-1})
$x_{g,i}$	mole fraction of species i in bulk gas phase
$x_{s,i}$	mole fraction of species i in gas at catalyst surface
z	axial position (m)
$\vec{\theta}$	vector of surface coverages

the absence of sulfur, substantial recovery of the overall catalytic activity was observed, which was attributed to sulfur's ability to migrate along the catalyst support, driven by a higher stability of the sulfate species on the oxide support [6].

To understand the effect of SO_2 on Pt/γ-Al_2O_3 activity, a number of research groups have investigated the interaction of alumina with SO_2 [7–14]. According to Datta et al. [7], the SO_2 adsorption process on γ-Al_2O_3 initially involves adsorption either at Lewis acid sites (coordinately unsaturated aluminum atoms) or at Lewis base sites (exposed oxygen atoms). Adsorption at Lewis acid sites gives rise to relatively weakly held SO_2 whereas interaction with the Lewis base sites leads to chemisorbed SO_2. Dalla Lana et al. [9] studied SO_2 adsorption on γ-Al_2O_3 and proposed an adsorption mechanism where the most likely mode involved interaction between oxygen atoms of the SO_2 molecule and oxygen vacancies on the alumina surface. According to their results, the oxygen vacancies were the only type of adsorption sites on the surface, but with a large distribution of binding energies due to the different atomic arrangements. They also found that SO_2 chemisorption was an activated process and the chemisorbed SO_2 was stable up to 602 °C. Nam and Gavalas [10] also suggested that there is a distribution of SO_2 adsorption sites on alumina and their relative strengths vary depending on pretreatment temperatures.

Mitchell et al. [12] observed sulfate species formation between 150 and 300 °C, even in the absence of gas-phase oxygen. SO_2 adsorption on under-saturated oxygen ions (less negatively charged compared to O^{2-} anions in the bulk of alumina) was suggested as a possible mechanism for surface sulfate formation [13]. Saur et al. [14] found that in the absence of OH groups or water, the surface sulfate formed during adsorption of SO_2 on alumina or titania has a tridentate structure, i.e. $(M_3O_3)S=O$ (with M representing Al or Ti), whereas in the presence of H_2O or excess surface OH groups, it can be converted to a bidentate sulfate. In another study, formation of two SO_4^{2-} species on alumina was reported: i) a well-dispersed surface species for concentrations up to 1.2×10^{14} ion/cm^2, and ii) bulk-like or subsurface compounds with further addition of SO_4^{2-} ions [15]. Surface sulfates on alumina decompose at temperatures above 700 °C [15]. Bulk aluminum sulfate is even more stable with a decomposition temperature around 800–920 °C [14]. It has been reported that the sulfate decomposition temperature on Pt/γ-Al_2O_3 can decrease by about 200 °C [16].

Interactions between supported Pt catalysts and SO_2 have also been studied in the literature [16–19]. Dawody et al. [17] studied the effect of SO_2 on the NO_x storage performance of Pt/BaO/Al_2O_3 and BaO/Al_2O_3 catalysts. The presence of Pt enhanced the adsorption of SO_2 under all exposure conditions studied. However, there was no correlation between the total amount of adsorbed sulfur on the samples and the deactivation rate of the NO_x storage capacity. It was proposed that sulfur adsorption on the sites that were not necessarily important for the NO_x storage process could be a reason for this observation [17]. In another study [20], SO_2 interactions with supported Pt catalysts were compared to those with the bare support. Upon SO_2 reaction with Al_2O_3, SO_x^{2-} species formed on the surface, where the chemical nature of the surface species changed with the reaction temperature such that SO_3^{2-} was the main species at 200 °C, SO_4^{2-} became dominant at 400 °C, with a mixture of SO_3^{2-} and SO_4^{2-} present at intermediate temperatures. Upon Pt/Al_2O_3 exposure to SO_2, surface sulfate formation started at lower temperatures and the yield of SO_4^{2-} species was larger compared to that with the bare support, however all the sulfate formed resided on alumina, rather than Pt sites, attributed to the higher stability of sulfate species on the support. Formation of sulfide species (S^{2-}) on the Pt surface, with a lower binding energy compared to that for sulfite and sulfate species, was also observed in the absence of oxygen [20].

Light and medium duty diesel exhaust typically has a peak temperature of around 250–300 °C. We have shown in our previous work [21] that non-trivial SO_2 oxidation on Pt/γ-Al_2O_3 starts at around 250 °C which is on the high side of the temperature domain commonly seen in the exhaust. The lower concentration of the resulting SO_3 also implies lower H_2SO_4 formation. Hence, the DOC will be exposed to SO_2 and its impact could be important with regards to performance. To simplify our overall problem statement in this study, we made a few simplifications for the kinetic measurements conducted during the course of the work:

- SO_2 oxidation can be negligible during the adsorption of SO_2 on a diesel oxidation catalyst; this assumption was used to exclude O_2 in the feed conditions.
- Formation of H_2SO_4 is negligible in the operating window of interest; thus we excluded H_2O in the experiments, which also substantially improved the quality of the data specifically for the in-situ DRIFTS measurements.

This work is therefore focused on SO_2 impacts. In the present work, SO_2 storage and release on γ-Al_2O_3 and Pt/γ-Al_2O_3 were studied using temperature-programmed desorption (TPD) and in-situ DRIFTS measurements, with an ultimate goal of developing a kinetic model to characterize and predict SO_2 poisoning of a Pt/γ-Al_2O_3 DOC. The effect of SO_2 on γ-Al_2O_3 was separately studied to decouple the support effect. DRIFTS experiments were utilized to identify the surface species formed upon γ-Al_2O_3 and Pt/γ-Al_2O_3 exposure to SO_2. The data obtained were then used to develop a model that can predict SO_2 storage and release.

2. Experimental methodology

2.1. Catalyst and monolith reactor set up

The γ-Al_2O_3 and Pt/γ-Al_2O_3 catalysts used in this study were provided by Johnson Matthey in monolithic form. The Pt/γ-Al_2O_3 monolith had a platinum loading of 50 g/ft^3, an Al_2O_3 loading of 1.6 g/in^3, and a cell density of 325 channels/in^2. An Al_2O_3-coated monolith, also loaded with 1.6 g/in^3, was used in the experiments with just Al_2O_3 evaluated. A monolithic core of 1.98 cm diameter and 2 cm length was used in the flow reactor system for each TPD experiment. The catalyst sample was inserted into a quartz tube reactor and small glass tubes, 2.5 mm ID and 3 mm OD, were

placed upstream of the sample to improve mixing and uniformity of the gas flow. The reactor assembly was placed in a temperature controlled furnace. For temperature measurements, three thermocouples were inserted at different locations inside the reactor. One thermocouple was located upstream of the catalyst, the two others were placed inside the sample, one close to the inlet face and the other close to the outlet face, all radially centered. MKS mass flow controllers were used to meter the gas flow rates and to set the desired gas concentrations. The inlet and outlet gas lines were heated to 150–200 °C in order to enhance temperature uniformity of the monolith and to prevent deposition of sulfur species in the lines. A MKS MultiGas MG-2030 FT-IR analyzer was used for the gas phase concentration measurements in the TPD experiments. The instrument was set to measure a data point every 0.5 s at a resolution of 0.5 cm^{-1} and the outlet gas concentrations were measured using SO_2 and SO_3 calibration methods developed in-house [21].

2.2. Temperature programmed desorption (TPD) experiments

Since the TPD experiments involved high temperature excursions, the monolith samples were removed after each experiment and replaced with a fresh sample to eliminate any doubt regarding catalyst degradation. Prior to each TPD experiment, the sample was hydrothermally aged at 710 °C for 4 h with a gas flow of 5% water, 10% oxygen, balanced with N_2. The reactor was then cooled down to the desired adsorption temperature while purging with N_2. Each TPD experiment was conducted in three phases. During the first phase, the adsorption phase, the catalyst was exposed to a constant concentration of SO_2 for 3 h, by which time the outlet concentration reached the inlet value, indicating that the surface was saturated at the given temperature. In the second phase, SO_2 was turned off and the sample was purged with N_2 for 10 min to desorb any loosely bound species. This phase was ended after 10 min, even if the outlet SO_2 concentration may not have reached 0 ppm. In the third phase, the catalyst was heated in N_2, at 20 °C/min, from the saturation temperature to ~920 °C, which based on sulfur mole balance calculations for each TPD experiment resulted in complete removal of the adsorbed sulfur species. The same TPD protocol was performed with an empty reactor to verify inlet concentration profiles and the lack of any adsorption in the lines. All aging and TPD experiments were conducted at a total flow rate of 2.64 L/min, corresponding to a space velocity of 25,000 h^{-1}.

2.3. In situ DRIFTS experiments

DRIFTS was used to characterize the species formed during SO_2 adsorption at two different temperatures (150 °C and either 400 °C or 450 °C), which were chosen based on the SO_2 desorption data obtained during the TPD experiments. Samples for DRIFTS were prepared by scraping the washcoat from the γ-Al_2O_3 and Pt/γ-Al_2O_3 monolith samples after they were hydrothermally aged, and the scrapings were separated from the cordierite substrate. Traces of the substrate material in the obtained washcoat powder may be present. The powder was pressed into a 60 mg pellet of 6.5 mm diameter and loaded in Harrick Scientific Praying Mantis reaction chamber. A fresh sample was used for each test.

According to Datta et al. [7], SO_2 adsorption is strongly affected by the presence of OH groups so that alumina samples with different degrees of dehydroxylation have different adsorption characteristics and thus IR spectra. To minimize the changes in the sample spectra due to the rearrangement of hydroxyl groups and to desorb any physisorbed water left on the surface, the sample was heated at 400 °C in He for 2 h prior to each DRIFTS experiment. After the pretreatment the reaction cell was set at the target adsorption temperature with He flowing and the background was collected after holding the sample at this temperature for at least 1 h until no variation was observed between spectra. SO_2 adsorption was performed by exposing either the γ-Al_2O_3 or Pt/γ-Al_2O_3 sample to 100 ppm SO_2 for 1 hour, which provided enough time for saturation. The DRIFTS cell was then purged with He for 30 min to remove the remaining SO_2 from the gas phase as well as to desorb weakly adsorbed species from the surface. The data were collected in the spectral range of 4000–400 cm^{-1} using a Nicolet 6700 IR spectrometer equipped with a MCT detector. All the experiments as well as the pretreatments were conducted with a total flow rate of 50 ml/min.

3. Model development

A two-phase transient model was developed for a single channel of the monolith, with the assumption that it can be considered a one-dimensional plug flow reactor. The following assumptions were used in the reactor model.

- The gas phase concentrations are quasi-equilibrated, thus there is no transient term in the species mole balance equation.
- No concentration gradient exists in the radial direction.
- The interactions between different adsorption sites are assumed to be negligible.
- A uniform temperature profile is assumed within the channel where $T_s \approx T_g \approx T_{g,in}$, thus the energy balance need not be solved. This assumption was verified with our temperature measurements where the difference between the inlet and outlet temperature was always below 4 °C.
- External mass transfer resistance is negligible, hence the species mole fraction on the catalyst surface is the same as the gas phase mole fraction: $x_{i,s} = x_{i,g}$.
- Internal mass transfer resistance in the washcoat pores is negligible.

The model equations consist of species balances in the gas phase and adsorbed species balances on the solid phase. The following set of governing equations was solved to obtain gas-phase SO_2 concentrations as well as adsorbed species surface coverages as a function of time and axial position within the channel:

Trace species conservation:

$$\frac{w_{in}}{A}\frac{\partial x_{g,SO_2}}{\partial z} = \sum_{j=1}^{nrct} a_{j,S_k} s_{ij} r_j \left(x_{g,SO_2}, \vec{\theta}\right) \quad (1)$$

Surface coverages:

$$\frac{\partial \theta_k}{\partial t} = F_k\left(T_s, \vec{c}_s, \vec{\theta}\right) \quad (2)$$

Site balance for each adsorption site:

$$\sum_i \theta_i = 1 \quad (3)$$

Note that in Eq. (1), r_j represents the individual reaction rates involved in SO_2 adsorption and release into the gas phase, which is calculated based on the proposed multi-site adsorption mechanism (described in Section 4.2.3). The reaction rate for SO_2 adsorption and desorption on each site is multiplied by the corresponding site density involved in that reaction, i.e. a_j,S_k. As shown in Eq. (2), the surface coverages on each site change with time due to adsorption, desorption or reaction taking place on that site; this in turn is a function of temperature, the SO_2 gas-phase concentration and surface coverages. In order to calculate the empty site coverage on each adsorption site, the site balance equation was considered for each adsorption site. The equations were solved in Matlab using ode15s for coverage equations, and ode23tb for the species equations after

suitable scaling. The variables involved in the above equations are all defined in the Nomenclature section.

4. Results and discussion

4.1. Temperature programmed desorption (TPD) results

TPD data obtained from the γ-Al_2O_3 and Pt/γ-Al_2O_3 samples after SO_2 exposure are shown in Fig. 1. A separate experiment was run with an empty reactor, and those data are displayed along with the TPD data to demonstrate the inlet concentration profiles. A mole balance analysis was performed to ensure all sulfur stored on the catalyst during the adsorption phase was released from the sample during the TPD. The mole balance errors as well as the SO_2 adsorbed amounts for both samples are listed in Table 1. Here, a positive error refers to some amount of sulfur left on the catalyst or measurement error, whereas a negative error would be measurement error. The sulfur loadings were calculated based on the desorbed amount during the TPD phase, i.e. not including the weakly adsorbed species released during the N_2 purge phase. It should be mentioned that during all the TPD experiments, SO_3 and H_2SO_4 concentrations were also monitored and neither was observed. As shown in Table 1, the small values of the mole balance errors support the accuracy of the TPD results. The relative similarity in the amount of adsorbed SO_2 when comparing γ-Al_2O_3 and Pt/γ-Al_2O_3 demonstrates the significance of the support in storing SO_2, as previously reported in the literature [2,5,14].

According to Waqif et al. [11], $Al_2(SO_4)_3$ is stable up to 800 °C and decomposes to γ-Al_2O_3 upon heating to higher temperatures. Therefore in the γ-Al_2O_3 TPD profile (Fig. 1), the peak corresponding to the highest temperature, i.e. above 850 °C, was assigned to bulk $Al_2(SO_4)_3$; and we have designated this species/peak as SO_2-S4. The large, lower temperature peak was considered as a combination of two desorption peaks, hereafter denoted as species SO_2-S1 and SO_2-S2. Similar surface species were identified in the case of SO_2 TPD from Pt/γ-Al_2O_3, however, the presence of Pt substantially increases the relative amounts of the more stable species. As shown in Fig. 1, the sharp peak centered at ~250 °C was again present (SO_2-S1) and the shoulder of this peak in the temperature range of 400–500 °C also (SO_2-S2). A third peak centered at 600 °C was also observed and is assigned as SO_2-S3, which was not obvious in the alumina TPD data. The high temperature peak is again bulk aluminum sulfate (SO_2-S4). The sulfur loadings obtained for both γ-Al_2O_3 and Pt/γ-Al_2O_3, are listed in Table 1. As shown in Fig. 1, the bulk sulfate peak in the TPD profile of Pt/γ-Al_2O_3 was shifted toward lower temperatures compared to that in the case of alumina. This is likely due to Pt facilitating decomposition of sulfates so that the decomposition occurs more readily compared to the same species on alumina [16].

4.2. Surface species identification using DRIFTS

DRIFTS was used to identify the nature of the surface sulfur species adsorbed on γ-Al_2O_3 and Pt/γ-Al_2O_3. SO_2 adsorption experiments were performed with each sample at two different temperatures, selected based on the desorption or decomposition temperatures observed in the TPD experiments (Section 4.1).

4.2.1. SO_2 adsorption on γ-Al_2O_3 DRIFTS results

DRIFTS spectra collected after saturating the sample with SO_2 for 60 min, and after further purging the sample with He for an additional 30 min to remove loosely bound species, are shown in the top spectra of each panel in Fig. 2. The spectrum labeled as "SO_2 saturated-150C" was recorded after 60 min exposure to 100 ppm SO_2 at 150 °C and the "Purged with He-150C" spectrum was collected 30 min after turning off the SO_2 flow, thus just purging with He. No significant difference was observed between the two spectra in the low wavenumber range, i.e. below 1800 cm^{-1}, in the presence and then absence of SO_2 in the gas. It should be noted that the characteristic bands of sulfur species on γ-Al_2O_3 in the IR spectra are mostly located at wavenumbers below 1800 cm^{-1}, therefore we have focused on this region in our analysis. The broad band in the range of 1000–1100 cm^{-1} represents surface sulfite species resulting from the interaction of SO_2 with oxygen sites in γ-Al_2O_3 [8]. The shoulder on the sharp peak in the range of 1300–1340 cm^{-1} is due to the presence of weakly adsorbed SO_2 on Al^{n+} Lewis acid sites [12]. The feature at 1267 cm^{-1} can be assigned to molecular SO_2 adsorbed on Al sites which are acidic and therefore not as strong as the basic oxygen sites [7]. The small features at 1585 and 1609 cm^{-1} are attributed to the sulfite species coordinated on Lewis acid sites (i.e. Al^{n+}), and the negative peak at 3742 cm^{-1} originates from hydroxyl groups on the alumina surface that were covered by sulfite/sulfate species. The small band located at 2965 cm^{-1} is assigned to a H-SO_3^- vibration, indicating bisulfite (HSO_3^-) formation via SO_2 interaction with residual hydroxyl groups [22]. The H-SO_3^- species may also contribute to the bands in the 1100–1200 cm^{-1} range, as well as to the sharp peak at 1267 cm^{-1} [22]. During the DRIFTS experiments on both γ-Al_2O_3 and Pt/γ-Al_2O_3, a broad band in the 3000–3650 cm^{-1} frequency range was always observed. This peak formed, and consistently increased after SO_2 was introduced into the system. As shown in Fig. 2, the intensity of this band significantly decreased after SO_2 was removed from the gas-phase and the sample was purged with He. This is explained by the interaction of SO_2 with surface hydroxyls leading to the formation of water and bisulfite species (HSO_3^-), according to the reaction pathway proposed by Zhao et al. [23]:

$$SO_2(g) + [OH^-] - Al(s) \rightarrow [HSO_3^-] - Al(s) \quad (4)$$

$$SO_2(g) + 2[OH^-] - Al(s) \rightarrow [SO_3^{2-}] - Al(s) + H_2O \quad (5)$$

As shown in Fig. 2, during the He purge some water was removed from the surface, resulting in a significant decrease in this broad band's intensity.

In order to study the effect of temperature on the nature of the adsorbed species, a similar experiment was performed with γ-Al_2O_3 with adsorption at 450 °C. This temperature was selected based on the TPD results, where the data suggested that one of the adsorbed species completely desorbed by 450 °C (Fig. 1), while remaining species were still present on the surface. The DRIFTS spectrum after 60 min SO_2 adsorption at 450 °C is shown as the bottom spectrum in Fig. 2. Interestingly, a new feature appeared at 450 °C, whereas the sharp peak at 1267 cm^{-1} was not apparent. This indicates that the first desorption peak in the TPD experiments (SO_2-S1) was associated with SO_2 attached to Al sites, with contribution from bisulfite (HSO_3^-) possible. The new feature around 1350 cm^{-1} was assigned to surface sulfate species, which was accompanied by the growth of the broad peak in the 950–1100 cm^{-1} range. The peak located at 1350 cm^{-1} is the characteristic band of surface sulfates, which we also observed when the catalyst was exposed to SO_2 and O_2 (not shown for brevity). The broad feature in the 950–1100 cm^{-1} range was attributed to the cooperative effects of surface sulfites and sulfates [23]. According to the adsorption mechanism proposed by Zhao et al. [23], when O_2 is present in the gas phase, it can adsorb on the surface, forming surface-active oxygen thereby facilitating further oxidation of bisulfite and sulfite species to sulfate. According to our DRIFTS results, the participation of surface oxygen, either originating from residual gas-phase O_2 or from the molecular structure of alumina, in the formation of surface sulfate became important upon heating the sample to 450 °C. Thus, sulfate formation on γ-Al_2O_3 is apparently an activated process. These DRIFTS results thus demonstrate that SO_2 can adsorb in a molecular state on Al sites or as surface sul-

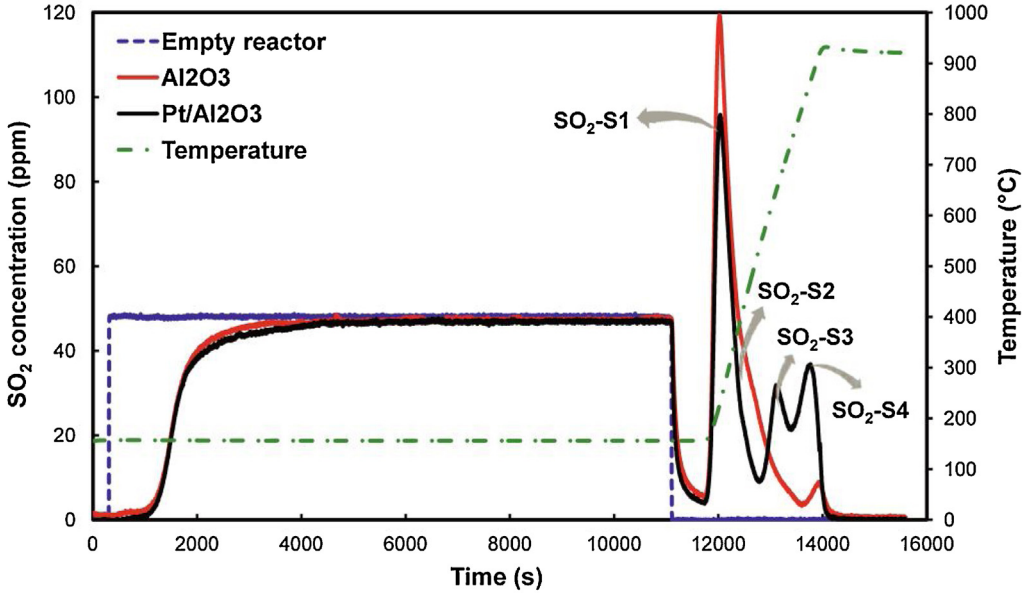

Fig. 1. SO_2 concentrations measured during adsorption followed by TPD with γ-Al_2O_3 and Pt/γ-Al_2O_3. Conditions during saturation: SO_2 inlet concentration = 48 ppm, temperature = 157 °C.

Table 1
SO_2 adsorption on γ-Al_2O_3 and Pt/γ-Al_2O_3.

Sample	Mole balance error (%)	SO_2 adsorbed (μmol)	BET surface area (m^2/g)	SO_2 loading on the washcoat (μmol/m^2)
γ-Al_2O_3 coated monolith	−1.3	141	101.09 ± 0.26	2.26
Pt/γ-Al_2O_3 coated monolith	0.4	158	94.69 ± 0.39	2.45

fite species on O^- sites, with some degree of conversion to sulfate species at higher temperatures.

4.2.2. SO_2 adsorption on Pt/γ-Al_2O_3 DRIFTS results

In order to identify the surface species on Pt/γ-Al_2O_3, the sample was exposed at 150 °C to 100 ppm SO_2 diluted with He. The DRIFTS spectrum recorded after 60 min SO_2 exposure at 150 °C is shown in Fig. 3. As can be observed in the top spectrum in Fig. 3, the IR bands are similar to those obtained for SO_2 adsorption on γ-Al_2O_3 at this temperature. The broad band at 1066 cm^{-1} represents surface sulfite and the sharp feature at 1260 cm^{-1} is SO_2 adsorbed on Al sites. The peak at 2964 cm^{-1} is attributed to bisulfite (HSO_3^-) with its accompanying features contributing to the peaks at 1260, 1189 and 1123 cm^{-1} wavenumbers [22]. The negative peaks at 1455 and 1585 cm^{-1} appeared as a result of the interaction of the adsorbed species with Lewis acid sites and the

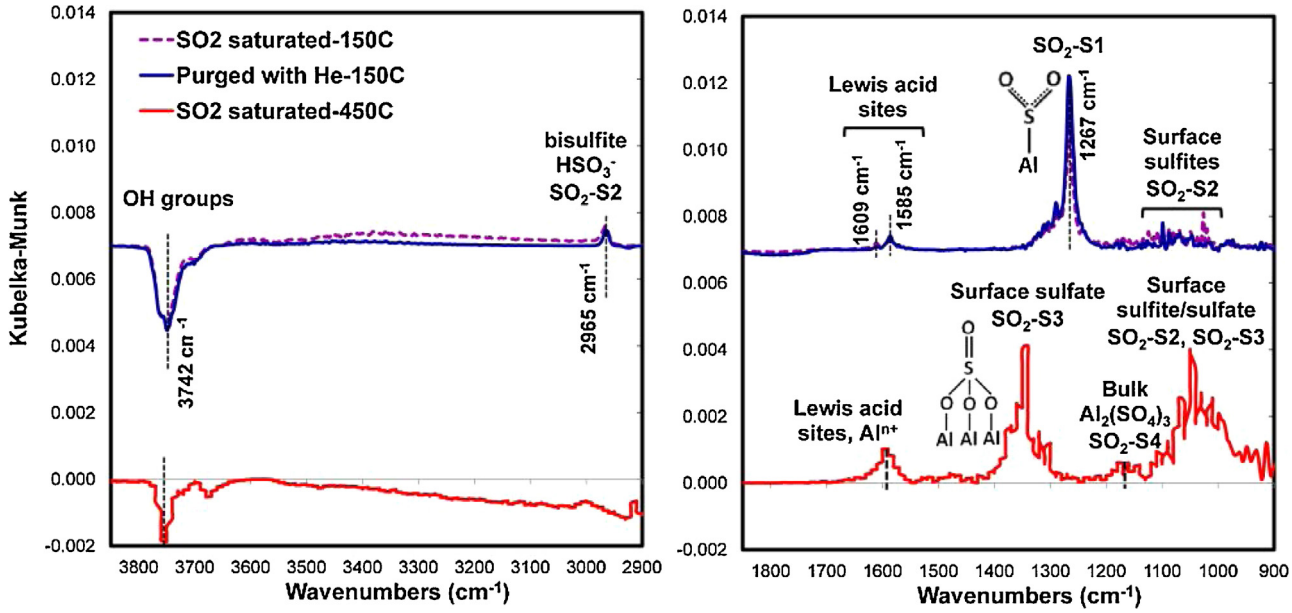

Fig. 2. Comparison between the DRIFTS spectra of γ-Al_2O_3 after exposure to 100 ppm SO_2 for 60 min at 150 °C (top spectra) and 450 °C (bottom spectra). The 450 °C spectrum has been multiplied by a factor of 5.

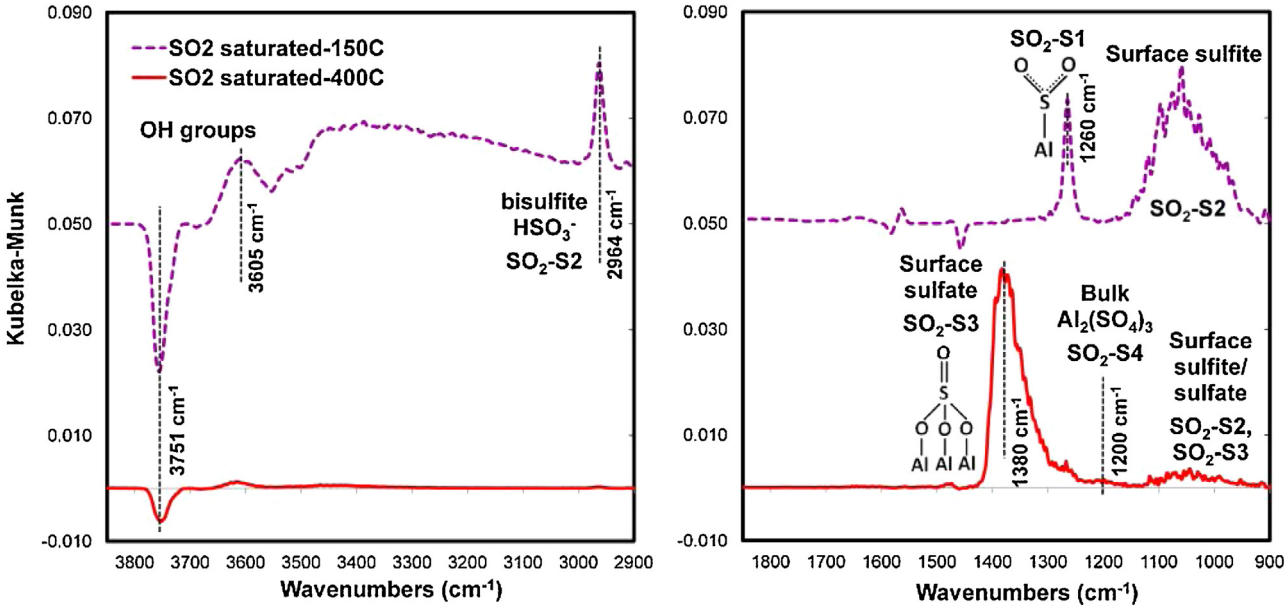

Fig. 3. Comparison between the DRIFTS spectra of Pt/γ-Al_2O_3 after exposure to 100 ppm SO_2 for 60 min at 150 °C (dashed line) and 400 °C (solid line). The 150 °C spectrum has been multiplied by a factor of 10.

Table 2
Surface species identified using DRIFTS and the corresponding naming convention.

IR frequency	Site	Naming convention	Reference
1267 cm^{-1}	Molecular SO_2 on Al	SO_2-S1	7
1300–1340 cm^{-1}	SO_2 adsorbed on Lewis acid sites (Al^{n+})	SO_2-S1	12
1066 cm^{-1}	Surface sulfite	SO_2-S2	12
2965 cm^{-1}	Bisulfite (HSO_3^-)	SO_2-S2	22
1070, 1380 cm^{-1}	Surface sulfate	SO_2-S3	10
1180–1200 cm^{-1}	Bulk aluminum sulfate	SO_2-S4	11

large negative peak at 3755 cm^{-1} was due to sulfur oxide interactions with the basic hydroxyl groups [22]. The broad features observed in the high frequency range, i.e. 2000–3500 cm^{-1}, could be due to the small amounts of physisorbed water produced as a result of SO_2 interaction with hydroxyl groups, as described earlier.

The DRIFTS spectrum obtained after exposure of Pt/γ-Al_2O_3 to 100 ppm SO_2 at an adsorption temperature of 400 °C is shown in Fig. 3. Again, the choice of 400 °C was based on Pt/γ-Al_2O_3 TPD results, where the first desorption peak ended at this temperature. Comparison between the two spectra collected at 150 °C and 400 °C reveal that an intense band at 1380 cm^{-1} appeared when SO_2 was adsorbed at 400 °C. In a study performed by Saur et al. [14], a feature at 1386 cm^{-1} in the IR spectra of sulfated Al_2O_3 was assigned to the terminal S=O bond of a tridentate surface sulfate species on Al_2O_3, i.e. $(Al\text{-}O)_3S{=}O$. Such a molecular structure for surface sulfates was similarly described for sulfated Al_2O_3 and TiO_2 [11]. There is a very small, broad feature at 1200 cm^{-1} in the 400 °C spectrum, which was not present at 150 °C. This band could be assigned to bulk aluminum sulfate, which is formed on alumina at high sulfur loadings and high enough temperatures. The rest of the features in the 400 °C spectrum are the same as those present at 150 °C, i.e. surface sulfite (1066 cm^{-1}), SO_2 adsorbed on Al sites (1260 cm^{-1}) and bisulfite (2964 cm^{-1}), however with their relative amounts compared to the surface sulfates being significantly lower at this temperature. Upon heating the sample to 600 °C, no significant change was observed in the surface sulfate peaks in the DRIFTS spectra, suggesting that the surface species formed at 400 °C are still stable at such a high temperature. 600 °C was the limit of the DRIFTS cell used.

One of the major differences between the spectra obtained from the Pt/γ-Al_2O_3 and γ-Al_2O_3 samples was the significant amount of surface sulfate formation at high temperatures (400 °C) in the Pt/γ-Al_2O_3 case. Based on these results, and in comparison with the TPD data where there was a more significant SO_2-S3 feature on Pt/Al_2O_3 vs Al_2O_3, we designated SO_2-S3 as surface sulfates. Furthermore, the presence of sulfite species in the DRIFTS, and with sulfate species being more stable than sulfite species, we designated the SO_2-S2 species as sulfites. A list of surface species along with their assigned naming convention, used in the modeling section, is shown in Table 2.

The increased amount of the surface sulfate and bulk sulfate observed for the Pt-containing catalyst, compared to alumina, indicates a promoting effect of Pt in sulfate formation as well as on the spillover of the surface sulfates to the bulk. In other words, Pt influences the catalyst sulfation through two different pathways: i) facilitates the oxidation of sulfite species to sulfates; ii) increases the mobility of the sulfur species from the surface to the bulk. The desorption pattern was also affected by Pt, where the bulk sulfates were decomposed with SO_2 release at lower temperatures compared to alumina. The reason could be the increased mobility of the adsorbed species and the reverse spillover of sulfates from bulk to the alumina surface. Metal-support interactions can also lead to the modification of the active sites and the formation of new adsorption sites [24]. Therefore, another reason for the observed shift in the desorption temperature of the peaks could be due to Pt-induced modification of the adsorption sites in the Pt-containing sample.

4.2.3. Surface reaction scheme

Multiple desorption peaks were observed in the TPD experimental results with γ-Al_2O_3 and Pt/γ-Al_2O_3, as shown in Fig. 1. Different

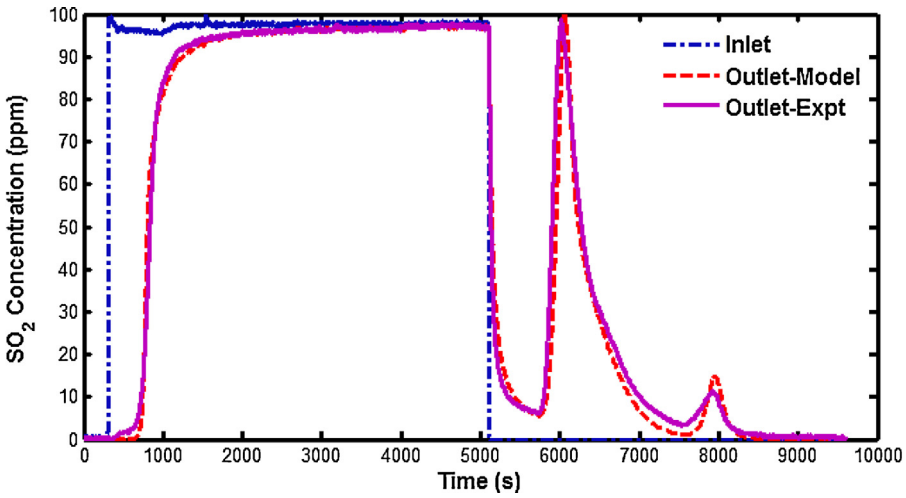

Fig. 4. Comparison of kinetic model fitting and experimental data for SO_2 TPD on γ-Al_2O_3. Saturation conditions: 98 ppm SO_2, 157 °C. Model parameters: Total site density: a_j = 23 mol site/m^3 monolith; Contribution of each site: $a_{j,S1} = 0.39a_j$, $a_{j,S2} = 0.55a_j$, $a_{j,S4} = 0.06a_j$.

Table 3
Reaction steps and rate expressions for SO_2 adsorption/desorption on/from γ-Al_2O_3.

Reaction	Reaction rate expression
$SO_2 + S1 \overset{1,2}{\leftrightarrow} SO_2 - S1$	$r_1 = A_1\exp(-E_1/RT)[SO_2]\theta_{S1}$ $r_2 = A_2\exp\left(-E_2\left(1-\alpha_1\theta_{SO_2-S1}\right)/RT\right)\theta_{SO_2-S1}$
$SO_2 + S2 \overset{3,4}{\leftrightarrow} SO_2 - S2$	$r_3 = A_3\exp(-E_3/RT)[SO_2]\theta_{S2}{}^3$ $r_4 = A_4\exp\left(-E_4\left(1-\alpha_2\theta_{SO_2-S2}\right)/RT\right)\theta_{SO_2-S2}{}^3$
$SO_2 - S2 + S4 \overset{5,6}{\leftrightarrow} SO_2 - S4 + S2$	$r_5 = A_5\exp(-E_5/RT)\theta_{SO_2-S2}{}^3\theta_{S4}$ $r_6 = A_6\exp(-E_6/RT)\theta_{S2}{}^3\theta_{SO_2-S4}$

surface species formed during SO_2 adsorption were characterized using the combined DRIFTS and TPD data, leading to the reaction scheme proposed here. A three site reaction scheme was proposed for SO_2 adsorption and desorption on/from γ-Al_2O_3, as shown in Table 3, with S1, S2 and S4 representing different adsorption sites. It should be mentioned that we originally considered a four site mechanism for SO_2 adsorption and desorption on/from γ-Al_2O_3 based on the DRIFTS and TPD data obtained with Pt/Al_2O_3, however since the contribution of the third site (i.e. S3) was insignificant in the Al_2O_3 TPD data, we chose to neglect the reaction step associated with S3 site in the mechanism and used a simplified three step reaction scheme for γ-Al_2O_3. In the three site mechanism shown in Table 3, S1 corresponds to Al sites on which SO_2 molecularly adsorbs, S2 corresponds to under coordinated oxygen atoms on the alumina matrix where surface sulfite forms and S4 represents the sites on which bulk aluminum sulfate forms. The physical interpretation of the adsorption sites and surface species along with the reaction kinetics assumed for each step will be further explained in Section 4.3.

A similar approach was applied to develop a reaction scheme for Pt/γ-Al_2O_3. The SO_2 TPD profile obtained from Pt/γ-Al_2O_3 is overlaid with that from γ-Al_2O_3 in Fig. 1. The desorption features from Pt/γ-Al_2O_3 are similar to those from γ-Al_2O_3, however, there was a larger contribution from bulk sulfates. Also, unlike the γ-Al_2O_3 the TPD data from Pt/γ-Al_2O_3 showed four distinct desorption peaks. In essence, we propose four different sites for SO_2 storage and release on/from Pt/γ-Al_2O_3, viz. S1 (corresponding to Al sites where SO_2 is molecularly adsorbed), S2 (corresponding to under coordinated oxygen atoms on the alumina matrix where surface sulfite forms), S3 (corresponding to under coordinated oxygen atoms on the alumina matrix where surface sulfate forms) and S4 (sites on which bulk aluminum sulfate forms). The proposed kinetic scheme for Pt/γ-Al_2O_3 is shown in Table 4.

4.3. Modeling results

4.3.1. Kinetic model for SO_2 adsorption–desorption on γ-Al_2O_3

The TPD and DRIFTS results demonstrate that the alumina support plays a significant role in the storage/release behavior of SO_2 on Pt/γ-Al_2O_3. Thus, in the modeling work, we first focused on SO_2 adsorption–desorption on γ-Al_2O_3 and developed a transient kinetic model for this system. In the next step, a kinetic model was developed for Pt/γ-Al_2O_3, taking advantage of the information obtained from the model of the γ-Al_2O_3 system.

Based on our findings from the TPD and DRIFTS results from both samples, four adsorption sites were considered for SO_2 adsorption on γ-Al_2O_3 and Pt/γ-Al_2O_3. As observed in Fig. 1, the TPD results show no unambiguous evidence of the decomposition of surface sulfates (i.e. SO_3-S3) on the Al_2O_3 surface. We cannot however conclude they did not exist, only that if they were formed from SO_2 oxidation at the surface they just as quickly decomposed or formed bulk sulfate species. The contribution of bulk sulfates (i.e. SO_2-S4) is very small on the alumina surface and since bulk sulfate forms through migration of surface sulfate to the alumina bulk, a small contribution for the surface sulfate would also be expected. We initially attempted to model the SO_2 adsorption on γ-Al_2O_3 using a four site adsorption mechanism (the modeling results are presented in Supporting information) where the contribution for the S3 sites was 4% of the total site density. But, due to this small contribution by the S3 sites, we simplified the reaction scheme to a three site mechanism by neglecting the adsorption/desorption

Table 4
Reaction steps and rate expressions for SO_2 adsorption/desorption on/from Pt/γ-Al_2O_3.

Reactions	Reaction rate expression
$SO_2 + S1 \overset{1,2}{\leftrightarrow} SO_2 - S1$	$r_1 = A_1\exp(-E_1/RT)[SO_2]\theta_{S1}$ $r_2 = A_2\exp\left(-E_2\left(1-\alpha_1\theta_{SO_2-S1}\right)/RT\right)\theta_{SO_2-S1}$
$SO_2 + S2 \overset{3,4}{\leftrightarrow} SO_2 - S2$	$r_3 = A_3\exp(-E_3/RT)[SO_2]\theta_{S2}{}^3$ $r_4 = A_4\exp\left(-E_4\left(1-\alpha_2\theta_{SO_2-S2}\right)/RT\right)\theta_{SO_2-S2}{}^3$
$SO_2 + S3 \overset{5,6}{\leftrightarrow} SO_2 - S3$	$r_5 = A_5\exp(-E_5/RT)[SO_2]\theta_{S3}{}^3$ $r_6 = A_6\exp(-E_6/RT)\theta_{SO_2-S3}{}^3$
$SO_2 - S3 + S4 \overset{7,8}{\leftrightarrow} SO_2 - S4 + S3$	$r_7 = A_7\exp(-E_7/RT)\theta_{SO_2-S3}{}^3\theta_{S4}$ $r_8 = A_8\exp(-E_8/RT)\theta_{S3}{}^3\theta_{SO_2-S4}$

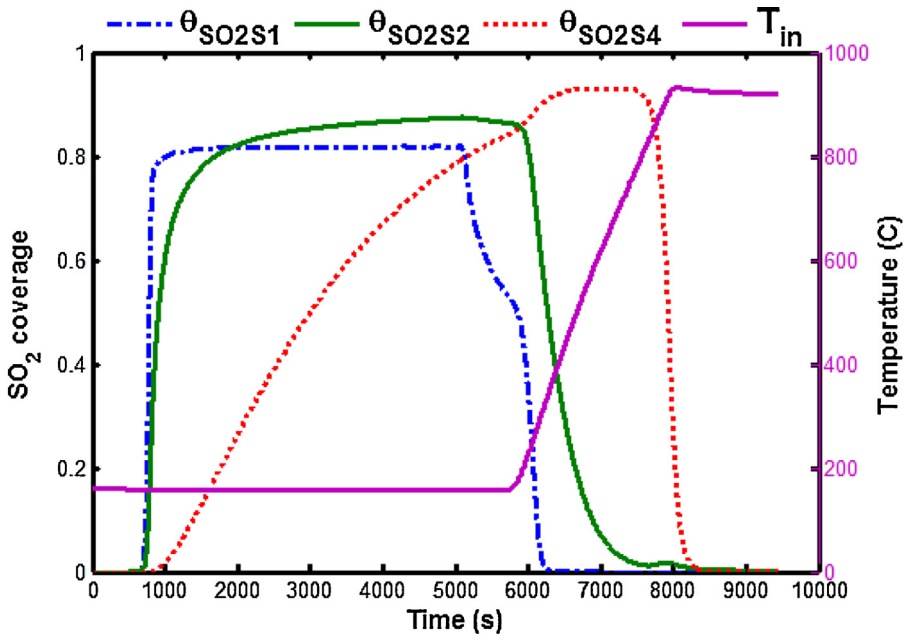

Fig. 5. Model-predicted coverages at the channel outlet as a function of time during SO_2 TPD on γ-Al_2O_3. Saturation conditions: 98 ppm SO_2, 157 °C. Site densities: total site density, a_j = 23 mol site/m^3 monolith; contribution of each site, $a_{j,S1} = 0.39a_j$, $a_{j,S2} = 0.55a_j$, $a_{j,S4} = 0.06a_j$.

step on the S3 site and considering its small contribution as part of the reaction step on the S2 sites. Therefore, a three site adsorption mechanism was proposed for the SO_2 adsorption/desorption on/from alumina as shown in Table 3. In the proposed reaction scheme, the second step is considered as the formation of surface sulfite species, i.e. on the S2 site, with any contribution from the surface sulfate species also included. The formation of the bulk sulfate species, the last mechanistic step, is proposed to be a spillover step to account for the migration of surface sulfite or sulfate species to the support.

We initially attempted to explain the γ-Al_2O_3 TPD data using first order kinetics for all the reaction steps. With first order kinetics, the SO_2 desorption from S1 and S4 sites could be predicted quite well, however, the model prediction showed a steep concentration decay during SO_2 desorption from S2, implying that the kinetic scheme was not capturing the formation and decomposition of surface sulfite species on the surface. Assuming a strong coverage dependency for the activation energy associated with SO_2 desorption from the S2 site did not result in any significant improvement. It turned out that using third order kinetics to model the reaction step(s) associated with the S2 site led to improved prediction of the experimental behavior. Based on our DRIFTS results, there is circumstantial physico-chemical support for the third order kinetics proposed in the reaction scheme. Strongly bound sulfite species are formed as a result of SO_2 interactions with basic oxygen ions or hydroxyl groups [12]. Bisulfite species also form due to the interaction between SO_2 and the most basic OH groups of alumina [25]. The relative population of these sulfite species depends on the termination oxygen ions and degree of dehydroxylation of the alumina surface [13]. Our DRIFTS data at low temperature (i.e. 150 °C) clearly showed the SO_2 interactions with hydroxyl groups on both γ-Al_2O_3 and Pt/γ-Al_2O_3 and subsequent release of water on the surface suggesting reaction (5) as a primary pathway for the formation of sulfite species. SO_2 adsorption on undersaturated oxygen ions (i.e. less negatively charged compared to usual O^{2-} ions) was also proposed in the literature as a possible mechanism for the formation of surface sulfate species on alumina [13]:

$$SO_2(g) + 2O^-(s) \rightarrow SO_4{}^{2-}(s) \quad (6)$$

Reactions (5) and (6) suggest non-first order kinetics for the sulfite and sulfate formation on the γ-Al_2O_3 and Pt/γ-Al_2O_3 surface. Furthermore, the IR bands observed at 1350 and 1380 cm^{-1} for the γ-Al_2O_3 and Pt/γ-Al_2O_3 sample, respectively, in our DRIFTS results suggest a tridentate structure for surface sulfate species on Al_2O_3, i.e. $(Al\text{-}O)_3S{=}O$, which would be consistent with third order kinetics from a mechanistic perspective. And with a significant surface coverage of O sites, SO_2 "finding" such a combination of sites would not be as statistically insignificant as most third order kinetics would typically be. However, the third order kinetics used do ultimately represent a best fit mathematically, with the characterization data only providing circumstantial support for higher order kinetics. Hence in the alumina model, first order kinetics were assumed for the coverages associated with the S1 and S4 sites, whereas third order kinetics were assumed for those related to the S2 site with coverage dependent desorption energies for S1 and S2.

The three site adsorption mechanism for the SO_2 adsorption/desorption on γ-Al_2O_3 was incorporated into the reactor model and the set of governing equations were solved to calculate the SO_2 gas-phase concentration as well as the surface coverages as a function of time and axial position within the monolith channel. A set of kinetic parameters including pre-exponential factors and activation energies was needed as an initial guess in order to solve the governing equations. Multiple TPD experiments with different ramp rates were performed on γ-Al_2O_3 to calculate the binding energies of the adsorbed species on each site, namely S1, S2, and S4, according to the method proposed by Falconer and Madix [26]. For each TPD data set, desorption peaks were deconvoluted to three peaks, assuming a Gaussian peak shape, and the desorption energies for SO_2-S1, SO_2-S2 and SO_2-S4 were calculated. Note, the method of heating rate variation provides accurate values when only one binding state occurs for each adsorbed species or when the peaks are not excessively broad [26]. Its application may be difficult in the case of substantially overlapping peaks or when a distribution of binding states exists for each adsorbed species, which is the case here for the SO_2-S2 and SO_2-S1. Hence, the activation energies calculated from the heating rate variation method were used as an estimate for solving the transient model and some of them were modified when needed to provide a better match to the experi-

Table 5
Kinetic parameter values used in the γ-Al_2O_3 model.

Reaction step	A_i	E_i(kJ/mol)
r_1	24 m^3 mol^{-1} s^{-1}	0
r_2	2.6×10^{10} s^{-1}	$115(1-0.15\theta_{SO2\text{-}S1})$
r_3	1.6×10^3 m^3 mol^{-1} s^{-1}	20
r_4	1.4×10^{11} s^{-1}	$170(1-0.27\theta_{SO2\text{-}S2})$
r_5	5 m^3 mol^{-1} s^{-1}	32
r_6	4.5×10^{14} s^{-1}	382

mental TPD data. The broad distribution of binding energies was taken into account using coverage dependent desorption energies for the SO_2-S1 and SO_2-S2 species on alumina.

As mentioned earlier, according to our DRIFTS results with alumina, S1 can be attributed to the Al sites where SO_2 is weakly adsorbed, with the first sharp peak in the TPD data representing desorption of these SO_2-Al species. The second peak which forms the broad shoulder is attributed to surface sulfite species. Ultimately, SO_2-S4 is the bulk aluminum sulfate which forms at higher temperatures and is stable up to 850 °C. Adsorption on S1 was assumed to be non-activated ($E_1 = 0$), since it readily formed on the alumina surface upon SO_2 adsorption at the lowest temperature employed in the DRIFTS experiments, 150 °C. On the other hand, the adsorption step on S2 and the spillover step on S4 were considered activated. According to the DRIFTS results, bulk sulfate formation required higher temperatures and thus resulted in a significant activation energy, while the activation energy for the sulfite formation reaction was relatively weak.

The pre-exponential factors as well as the coverage dependence of the desorption energies were tuned to fit the experimental data. The initial guesses for the pre-exponential factors related to the desorption steps were estimated based on typical values suggested by transition state theory (TST) [27]. The upper limits for the adsorption pre-exponential factors were calculated based on collision theory [28]. In order to impose thermodynamic constraint on the kinetic parameters, the entropy change for SO_2 adsorption was calculated based on the two extreme cases, i.e. localized vs. 2D gas adsorbate [29], as described in the Supporting information. The values of the pre-exponential factors were fitted such that the model-predicted entropy change lies within this range. An adsorption enthalpy of 350 kJ/mol was obtained for the SO_2-S4 species, which is in good agreement with the values reported in the literature for the bulk aluminum sulfate [30].

The model predictions along with the experimental data are shown in Fig. 4 with all the kinetic parameters employed in the model listed in Table 5. As shown in Fig. 4, the model with the fitted parameters is able to accurately predict the experimental data during both the SO_2 storage and release phases. It should be mentioned that, as described in the TPD experimental procedure, the adsorption phase was performed over a three-hour period to ensure the catalyst was completely saturated. However, in order to decrease the computational time required to run the transient model, the adsorption phase data set was decreased by eliminating a range of data where no significant change was observed in the outlet concentration. In doing so, a time period of 6000 s in length, within the saturation phase, was removed from the original experimental data set prior to solving the transient model. That is the reason why the adsorption phase in the modeling results appears shorter than that described in the TPD experimental procedure.

The model-predicted coverages at the channel outlet along with the catalyst temperature are shown as a function of time in Fig. 5. During the adsorption phase at 157 °C, SO_2 is adsorbed on the S1 and S2 sites leading to the formation of SO_2-Al and the surface sulfite species. The formation of the bulk aluminum sulfate starts later, as it is highly activated and also depends on the SO_2-S2 coverage according to our proposed mechanism. As a reminder, in the alumina model (Table 2), the formation of surface sulfate, which had a small contribution in TPD profile, is here considered along with surface sulfite (as SO_2-S2 species) and therefore the spillover step is modeled as S2 to S4. SO_2-S1 and SO_2-S2 reach saturation coverages of 0.82 and 0.87, respectively, at the end of the adsorption phase. When the SO_2 flow was stopped, some of the SO_2 adsorbed on the Al sites, i.e. SO_2-S1, desorbed in order to reach a new equilibrium state. Surface sulfites are more stable with a low desorption rate at this temperature, therefore the SO_2-S2 coverage drop due to desorption was not significant during this phase. As the temperature increased, the SO_2-S1 and SO_2-S2 coverages dropped, whereas the rate of SO_2-S4 formation increased resulting in a rapid increase in the bulk aluminum sulfate coverage. At 580 °C, bulk aluminum sulfate (SO_2-S4) reached a saturation coverage of 0.93 while the surface sulfite and sulfate coverages continued decreasing due to decomposition and SO_2 desorption into the gas phase. Bulk aluminum sulfate also started decomposing once the temperature reached 800 °C.

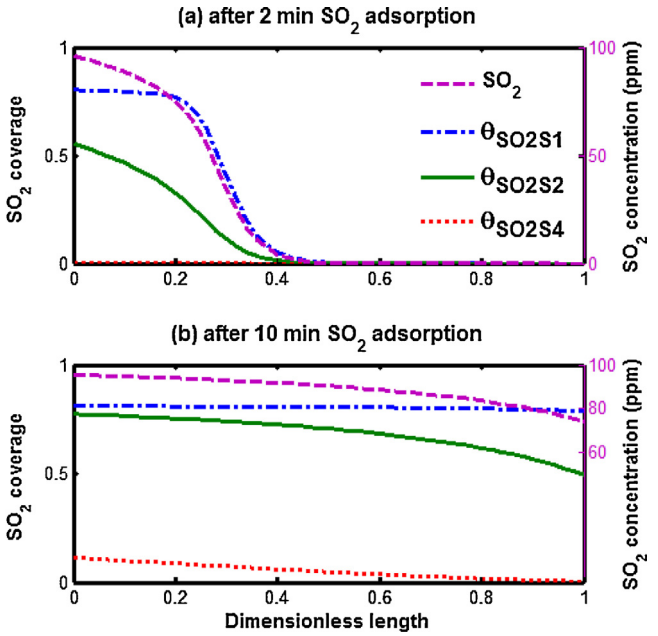

Fig. 6. Model-predicted coverages along a monolith channel during the SO_2 TPD experiment with γ-Al_2O_3. Saturation conditions: 98 ppm SO_2, 157 °C. (a) after 2 min SO_2 exposure, (b) after 10 min SO_2 exposure.

Surface coverages plotted as a function of channel length at two different times during the adsorption phase are shown in Fig. 6. The gas-phase SO_2 concentration is also shown. With increasing exposure time, the adsorption front moves progressively along the channel length as expected. With further exposure time, as shown in Fig. 6b, the coverage profile extends along the whole length of the channel leading to more uniform coverage profiles. Therefore, the model predicts the right trend, sulfur poisoning will affect catalyst activity in a non-uniform manner when evaluating the transient behavior of the system. Such non-uniform profiles can have a more significant role for very low SO_2 concentrations (e.g. 1 ppm), which are more realistic in terms of engine exhaust gas concentrations, where the progress of the poisoning front toward the back portion of the catalyst would take significantly longer than what we have shown here. For comparison, the model predicted coverages for such low SO_2 concentrations will be shown for the Pt/γ-Al_2O_3 sample, in Section 4.3.2.

4.3.2. Kinetic model for SO_2 adsorption–desorption on Pt/γ-Al_2O_3

A similar methodology was applied to develop the kinetic model for SO_2 adsorption and desorption on/from Pt/γ-Al_2O_3. In the case of Pt/γ-Al_2O_3, a four site mechanism was assumed, as described in

Table 4. Similar to the alumina model, S1 represents the Al sites, S2 is attributed to the sites on which surface sulfites and bisulfites are formed, S3 is attributed to the sites where surface sulfates are formed and S4 represents bulk aluminum sulfate species. Note that the DRIFTS and the TPD experiments showed significant formation of surface sulfate with a distinct desorption peak observed in the TPD data, as opposed to the γ-Al_2O_3 case and thus the formation of surface sulfates needed to be explicitly accounted for in the overall kinetic scheme here. We followed the same methodology for the development of the reaction kinetics as that followed for the γ-Al_2O_3 case. Again, third order kinetics were used for the S2 (i.e. surface sulfite) and S3 sites (i.e. surface sulfate) with the rest of the sites being first order. Linear coverage dependencies were considered for the desorption energies from the S1 and S2 sites. It should be mentioned that due to the small amount of the Pt sites on the catalyst compared to the alumina sites, and since the binding energy of sulfur species on Pt is lower than that on the weak alumina sites, none of the peaks are assigned to SO_2-Pt species. However, the presence of Pt influences the SO_2 storage/release pattern significantly by increasing the sulfation rate as well as the sulfate spillover from the surface to the bulk. Sulfide formation on Pt sites upon SO_2 exposure in the absence of oxygen is indeed possible according to the literature [20]. Our experiments were conducted in the absence of O_2 in the feed, however, the presence of residual oxygen (in ppm levels, <6 ppm based on measurement ability) in the gas stream could not be avoided. Since the characteristic IR frequencies of the Pt sulfide species are within the 488.9–583.6 cm^{-1} range [31], which is outside the region where the DRIFTS data could be collected, we were not able to identify sulfide species based on the DRIFTS results. But, due to the presence of residual oxygen in the feed, we assumed that the formation of PtS species is relatively negligible under our operating conditions.

The four-site mechanism for the SO_2 adsorption–desorption on Pt/γ-Al_2O_3 was incorporated into the set of governing equations. Some of the activation energies and coverage dependencies of the desorption energies were taken from the alumina model and used here. The rest of the kinetic parameters were optimized to describe the experimental data with thermodynamic constraints imposed upon the pre-exponential factors, using the same methodology employed in the case of γ-Al_2O_3. The model fitting results for the SO_2 adsorption/desorption on Pt/γ-Al_2O_3 and the experimental data are compared in Fig. 7 and the values of the kinetic parameters are listed in Table 6. As shown earlier in Fig. 1, the bulk sulfate peak in the TPD data of Pt/γ-Al_2O_3 was shifted toward lower temperatures compared to that in the case of alumina. This is due to Pt facilitating decomposition of sulfates so that the decomposition occurs more readily compared to the same species on alumina [19]. According to our reaction scheme, the bulk aluminum sulfate decomposition occurs through the reverse spillover of the bulk species to the surface which is promoted in the presence of Pt. The decomposition/desorption activation energy of 267 kJ/mol obtained from the Pt/γ-Al_2O_3 model verifies such a promoting effect of Pt on the kinetics of bulk aluminum sulfate decomposition. In addition, the lower activation energies obtained for the SO_2-S2 (surface sulfite) and SO_2-S3 (surface sulfate) formation on the Pt-containing catalyst compared to alumina indicates the promoting effect of Pt on SO_2 oxidation, thus a higher degree of sulfate formation on this catalyst.

Table 6
Kinetic parameter values used in the Pt/γ-Al_2O_3 model.

Reaction step	A_i	E_i(kJ/mol)
r_1	1.5 m^3 mol^{-1} s^{-1}	0
r_2	1.4×10^9 s^{-1}	$116(1–0.15\theta_{SO2\text{-}S1})$
r_3	25 m^3 mol^{-1} s^{-1}	10
r_4	1×10^{11} s^{-1}	$162(1–0.25\theta_{SO2\text{-}S2})$
r_5	4.5×10^2 m^3 mol^{-1} s^{-1}	18
r_6	9×10^{13} s^{-1}	263
r_7	0.27 s^{-1}	28
r_8	3×10^{10} s^{-1}	267

The model-predicted surface coverages were calculated for the channel outlet and shown as a function of time in Fig. 8. These results reveal that during the adsorption phase the S2 sites are filled first producing SO_2-S2 or the surface sulfite species. These species are formed through the interaction of SO_2 with electron deficient oxygen sites on the surface of alumina. The presence of Pt facilitates sulfite formation by decreasing the activation energy of the adsorption step on the S2 site. SO_2-S1 and SO_2-S3, representing SO_2-Al and surface sulfates respectively, also increase during the adsorption phase until they reach a saturation level. According to the model, the maximum coverages of 0.80, 0.90 and 0.77 were obtained at the end of the adsorption phase for SO_2-S1, SO_2-S2 and SO_2-S3, respectively. A similar trend to that observed in the case of alumina was observed during the desorption phase and the temperature ramp. The bulk sulfate coverage (SO_2-S4) gradually increased during the adsorption phase as a result of surface sulfate

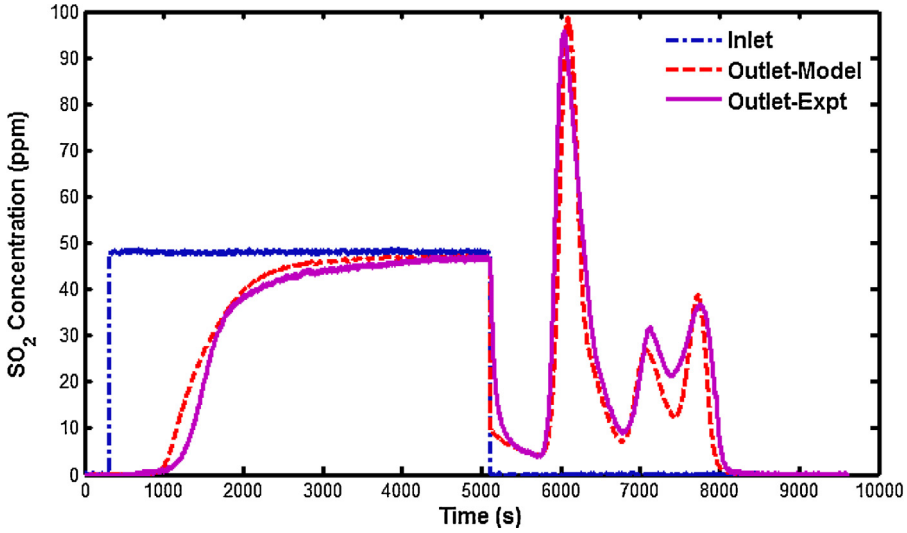

Fig. 7. Comparison of kinetic model fitting and experimental data for SO_2 TPD on Pt/γ-Al_2O_3. Saturation conditions: 48 ppm SO_2, 157 °C. Model parameters: Total site density: a_j = 30 mol site/m^3 monolith; Contribution of each site: $a_{j,S1} = 0.28a_j$, $a_{j,S2} = 0.27a_j$, $a_{j,S3} = 0.25a_j$, $a_{j,S4} = 0.2a_j$.

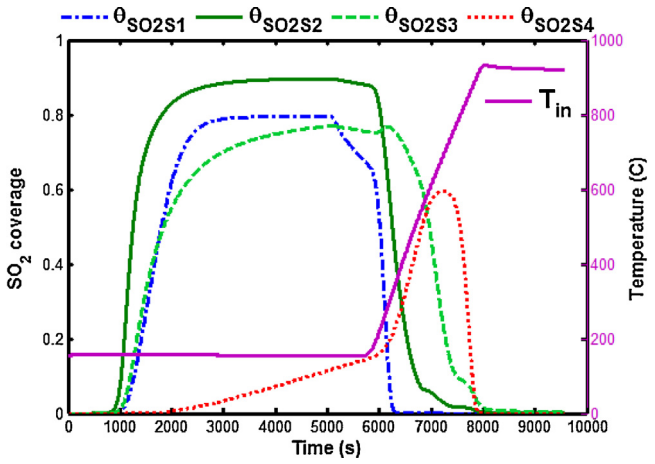

Fig. 8. Model-predicted coverages at the channel outlet as a function of time during the SO_2 TPD experiment with Pt/γ-Al_2O_3. Saturation conditions: 48 ppm SO_2, 157 °C. Site densities: total site density, a_j = 30 mol site/m^3 monolith; contribution of each site, $a_{j,S1} = 0.28a_j$, $a_{j,S2} = 0.27a_j$, $a_{j,S3} = 0.25a_j$, $a_{j,S4} = 0.2a_j$.

spillover to the bulk. The formation of bulk aluminum sulfate was accelerated during the temperature ramp until SO_2-S4 reached the maximum coverage of 0.59 at approximately 690 °C. Similar to the trend observed in the TPD profile, the surface of the Pt-containing catalyst is completely regenerated from the sulfur compounds at ~880 °C which is slightly lower than that observed for γ-Al_2O_3.

The surface coverages and the SO_2 gas-phase concentration at a specific time along the channel of the Pt/γ-Al_2O_3 monolith are shown in Fig. 9. The top panel (a) shows the coverage profile after 4 min SO_2 exposure and the bottom panel (b) shows the same profile after 20 min. Since the inlet SO_2 concentration in this case is 48 ppm, which is about half of the concentration employed in the alumina model, we have selected longer exposure times such that the cumulative amount of sulfur exposure are similar in the two cases. It should be mentioned that using the same SO_2 concentration and exposure time as those employed in the alumina model

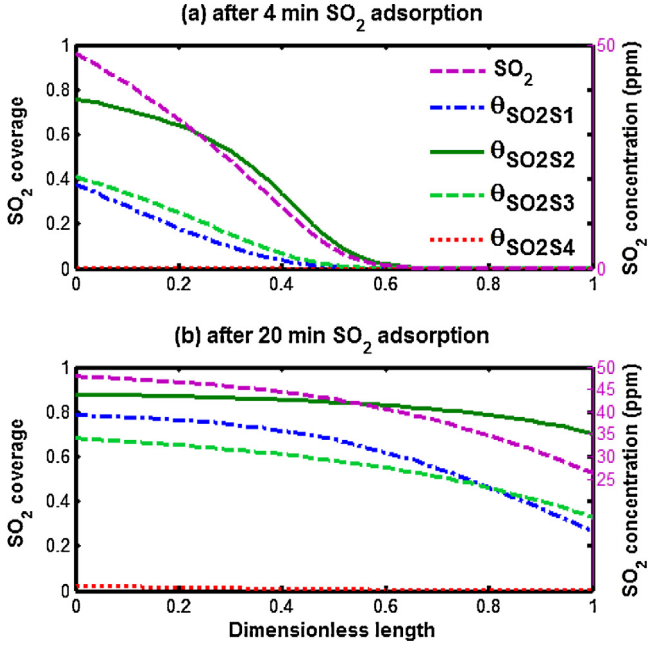

Fig. 9. Model-predicted coverages along a monolith channel during the SO_2 TPD experiment with Pt/γ-Al_2O_3. Saturation conditions: 48 ppm SO_2, 157 °C. (a) after 4 min SO_2 exposure, (b) after 20 min SO_2 exposure.

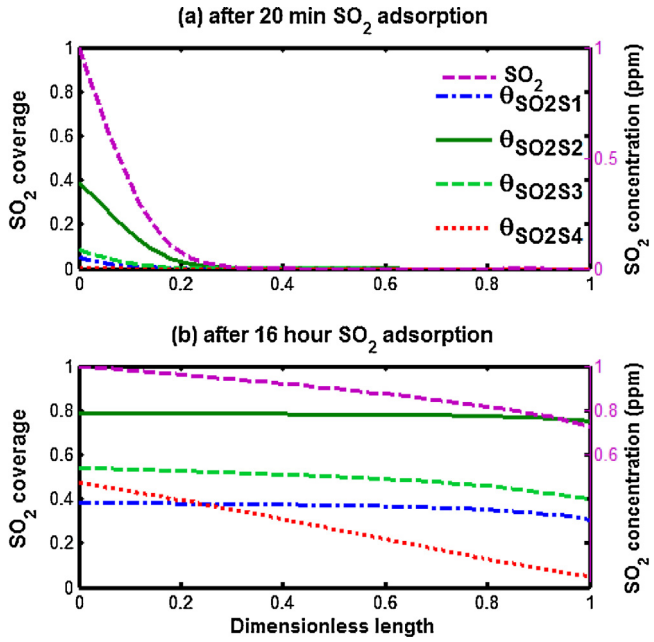

Fig. 10. Model-predicted coverages along a monolith channel for SO_2 adsorption on Pt/γ-Al_2O_3. Adsorption conditions: 1 ppm SO_2, 157 °C. (a) after 20 min SO_2 exposure, (b) after 16 h SO_2 exposure.

led to similar results to those reported here. As shown in Fig. 9a, a similar adsorption front is observed within the channel in the initial stage of the sulfur exposure. However, with Pt/γ-Al_2O_3 the oxygen sites in the alumina matrix, surface sulfite species, are covered first, with SO_2-Al and surface sulfates being formed subsequently. The back portion of the channel was not impacted after 4 min. After 20 min, as shown in Fig. 9b, the whole length of the channel would be affected by sulfur, with a more uniform profile of the surface coverages in the axial direction.

The surface coverages on Pt/γ-Al_2O_3 were also predicted under more realistic exhaust gas concentrations, where 1 ppm SO_2 was instead used in the feed. The model-predicted surface coverages and the SO_2 gas phase concentration at two specific times along the monolith channel are shown in Fig. 10. As shown in Fig. 10a, when the catalyst is exposed to 1 ppm SO_2 for 20 min, only 20% of the channel length is significantly covered by sulfur species. Similar to the results obtained with 48 ppm SO_2, surface sulfites are the most dominant surface species being formed in the initial stage of SO_2 exposure, followed by surface sulfates and SO_2-Al. Fig. 10b shows the model-predicted coverages after a 16 hour exposure to 1 ppm SO_2, which is equivalent to Fig. 9b in terms of cumulative amount of SO_2 exposure. After 16 h of SO_2 exposure, surface sulfites are the most dominant adsorbed species with a coverage close to the saturation level for the S2 sites. Surface sulfates and SO_2-Al are also uniformly distributed along the axial direction with a gradual increasing trend toward their saturation levels. It should be mentioned that the lower coverage of SO_2-Al relative to surface sulfates is due to the low SO_2 concentration. The formation of bulk $Al_2(SO_4)_3$ is more remarkable, compared to that observed for shorter sulfur exposure times, demonstrating the role of Pt in facilitating surface sulfate mobility and therefore enhanced spillover of sulfates from the surface into the bulk.

5. Conclusions

SO_2 adsorption/desorption on γ-Al_2O_3 and Pt/γ-Al_2O_3 was studied to predict sulfur storage and release on a Pt-based oxidation catalyst. The significant role of alumina, as a catalyst support, in

SO_2 storage was decoupled by also characterizing γ-Al_2O_3 samples. DRIFTS experiments were utilized to identify the surface species formed at different temperatures. According to the DRIFTS and TPD results, upon γ-Al_2O_3 exposure to SO_2, SO_2 interacts with aluminum and oxygen sites resulting in the formation of SO_2 adsorbed on Al sites, surface sulfites/sulfates as well as bulk aluminum sulfates. Based on these results, a three-site kinetic mechanism was proposed for SO_2 adsorption on γ-Al_2O_3 and a transient kinetic model was developed for a single channel of the monolith. A similar methodology was also applied in the Pt/γ-Al_2O_3 kinetic model development, where surface species similar to those observed on alumina were identified on the Pt/γ-Al_2O_3 catalyst, however with a higher contribution of the more stable species, indicating the promoting effect of Pt on surface sulfate formation as well as on spillover of surface sulfates into the bulk. Also, a distinct surface sulfate species was observed, which was not when characterizing only Al_2O_3. A four-site reaction mechanism was proposed for SO_2 adsorption/desorption on Pt/γ-Al_2O_3 and a transient kinetic model was again developed. The transient models were able to accurately predict the experimental behavior of the catalyst and verify intuitive trends. For example, in the initial stages of SO_2 exposure, only the front portion of the Pt/γ-Al_2O_3 catalyst is impacted by sulfur. As the exposure time increases, the poisoning front moves progressively along the channel leading to nearly uniform coverage profiles along the entire monolith channel. Model predictions showed that with 1 ppm SO_2, which is more realistic in terms of exhaust gas concentrations, the entire channel had similar steady state coverages over extended periods of time, i.e. approximately 16 h, in comparison to high concentration exposures at shorter time scales.

Acknowledgements

The authors gratefully acknowledge Cummins Inc for financial support and Johnson Matthey for the donated catalyst sample. We also thank MKS instruments for collaboration in the FT-IR sulfur calibration development.

Appendix A. Supplementary data

Supplementary data associated with this article can be found, in the online version, at http://dx.doi.org/10.1016/j.apcatb.2015.08.003.

References

[1] A. Russell, W.S. Epling, Catal. Rev. Sci. Eng. 53 (2011) 337–423.
[2] F.J. Gracia, S. Guerrero, E.E. Wolf, J.T. Miller, A.J. Kropf, J. Catal. 233 (2005) 372–387.
[3] Y.S. Kim, S.J. Lim, Y.H. Kim, J.H. Lee, H.I. Lee, Res. Chem. Intermed. 38 (2012) 947–955.
[4] O. Krocher, M. Widmer, M. Elsener, D. Rothe, Ind. Eng. Chem. Res. 48 (2009) 9847–9857.
[5] J.H. Pazmiño, J.T. Miller, S.S. Mulla, W. Nicholas Delgass, F.H. Ribeiro, J. Catal. 282 (2011) 13–24.
[6] J. Li, A. Kumar, X. Chen, N. Currier, A. Yezerets, SAE Tech. Pap. Series (2013), No. 2013-01-0514.
[7] A. Datta, R.G. Cavell, R.W. Tower, Z.M. George, J. Phys. Chem. 89 (1985) 443–449.
[8] C. Chang, J. Catal. 53 (1978) 374–385.
[9] I.G. Dalla Lana, H.G. Karge, Z.M. George, J. Phys. Chem. 97 (1993) 8005–8011.
[10] S.W. Nam, G.R. Gavalas, Appl. Catal. 55 (1989) 193–213.
[11] M. Waqif, O. Saur, J.C. Lavalley, S. Perathoner, G.J. Centi, Phys. Chem. 13 (1991) 4051–4058.
[12] M.B. Mitchell, V.N. Sheinker, C. Atlanta, V. Uni, M.G. White, J. Phys. Chem. 100 (1996) 7550–7557.
[13] M.Y. Smirnov, A.V. Kalinkin, A.V. Pashis, A.M. Sorokin, A.S. Noskov, K.C. Kharas, V.I. Bukhtiyarov, J. Phys. Chem. B 109 (2005) 11712–11719.
[14] O. Saur, M. Bensitle, A.B. Mohammed Saad, J.C. Lavalley, C.P. Tripp, B.A. Morrow, J. Catal. 99 (1986) 104–110.
[15] Y. Okamoto, T. Imanaka, J. Phys. Chem. 92 (1988) 7102–7112.
[16] D. Uy, A. Dubkov, G.W. Graham, W.H. Weber, Catal. Lett. 68 (2000) 25–32.
[17] J. Dawody, S. Magnus, L. Olsson, E. Fridell, J. Catal. 234 (2005) 206–218.
[18] F. Cabello Galisteo, R. Mariscal, M. López Granados, M.D. Zafra Poves, J.L.G. Fierro, V. Kröger, R.L. Keiski, Appl. Catal. B 72 (2007) 272–281.
[19] J.M. Jones, V.A. Dupont, R. Brydson, D.J. Fullerton, N.S. Nasri, A.B. Ross, A.V.K. Westwood, Catal. Today 81 (2003) 589–601.
[20] M.Y. Smirnov, A.V. Kalinkin, A.V. Pashis, I.P. Prosvirin, V.I. Bukhtiyarov, J. Phys Chem. C 118 (2014) 22120–22135.
[21] T. Hamzehlouyan, C.S. Sampara, J. Li, A. Kumar, W.S. Epling, Appl. Catal. B 152–153 (2014) 108–116.
[22] J. Garcia-Martinez, D. Cazorla-Amoro, A. Linares-Solano, Langmuir 18 (2002) 9778–9782.
[23] L. Zhao, X. Li, X. Quan, G. Chen, Environ. Sci. Technol. 45 (2011) 5373–5379.
[24] D.J. Fullerton, A.V.K. Westwood, R. Brydson, M.V. Twigg, J.M. Jones, Catal. Today 81 (2003) 659–671.
[25] J.C. Lavalley, A. Janin, J. Preud'homme, React. Kinet. Catal. Lett. 18 (1981) 85–88.
[26] J.L. Falconer, R.J. Madix, Surf. Sci. 48 (1975) 393–405.
[27] V.P. Zhdanov, Elementary Physicochemical Processes on Solid Surfaces, in: M.V. Twigg, M.S. Spencer (Eds.), Plenum Press, New York and London, 1991, p. 57.
[28] L. Olsson, B. Andersson, Top. Catal. 28 (2004) 89–98.
[29] C.T. Campbell, J.R.V. Sellers, J. Am. Chem. Soc. 134 (2012) 18109–18115.
[30] D.W. Johnson, P.K. Gallagher, J. Am. Ceram. Soc. 54 (1971) 461–465.
[31] B. Liang, X. Wang, L. Andrews, J. Phys. Chem. A 113 (2009) 3336–3343.